

Journal of Biomedical Optics

SPIEDigitalLibrary.org/jbo

Metabolism of HeLa cells revealed through autofluorescence lifetime upon infection with enterohemorrhagic *Escherichia coli*

Tatyana Yu. Buryakina
Pin-Tzu Su
Wan-Jr Syu
C. Allen Chang
Hsiu-Fang Fan
Fu-Jen Kao

Metabolism of HeLa cells revealed through autofluorescence lifetime upon infection with enterohemorrhagic *Escherichia coli*

Tatyana Yu. Buryakina,^{a*} Pin-Tzu Su,^{b*} Wan-Jr Syu,^b C. Allen Chang,^c Hsiu-Fang Fan,^d and Fu-Jen Kao^a

^aNational Yang-Ming University, Institute of Biophotonics, 155 Linong Street, Section 2, Taipei 11221, Taiwan

^bNational Yang-Ming University, Institute of Microbiology and Immunology, 155 Linong Street, Section 2, Taipei 11221, Taiwan

^cNational Yang-Ming University, Department of Biomedical Imaging and Radiological Sciences, 155 Linong Street, Section 2, Taipei 11221, Taiwan

^dNational Yang-Ming University, Institute of Life Sciences, 155 Linong Street, Section 2, Taipei 11221, Taiwan

Abstract. Fluorescence lifetime imaging microscopy (FLIM) is a sensitive technique in monitoring functional and conformational states of nicotinamide adenine dinucleotide reduced (NADH) and flavin adenine dinucleotide (FAD), main compounds participating in oxidative phosphorylation in cells. In this study, we have applied FLIM to characterize the metabolic changes in HeLa cells upon bacterial infection and made comparison with the results from the cells treated with staurosporine (STS), a well-known apoptosis inducer. The evolving of NADH's average autofluorescence lifetime during the 3 h after infection with enterohemorrhagic *Escherichia coli* (EHEC) or STS treatment has been observed. The ratio of the short and the long lifetime components' relative contributions of NADH increases with time, a fact indicating cellular metabolic activity, such as a decrease of oxidative phosphorylation over the course of infection, while opposite dynamics is observed in FAD. Being associated with mitochondria, FAD lifetimes and redox ratio could indicate heterogeneous mitochondrial function, microenvironment with bacterial infection, and further pathway to cell death. The redox ratios for both EHEC-infected and STS-treated HeLa cells have been observed and these observations also indicate possible apoptosis induced by bacterial infection. © 2012 Society of Photo-Optical Instrumentation Engineers (SPIE). [DOI: 10.1117/1.JBO.17.10.101503]

Keywords: bacterial infection; fluorescence lifetime imaging microscopy; staurosporine; apoptosis; metabolism; nicotinamide adenine dinucleotide reduced.

Paper 11747SS received Dec. 14, 2011; revised manuscript received Feb. 9, 2012; accepted for publication Mar. 2, 2012.; published online May 21, 2012.

1 Introduction

Autofluorescence spectroscopy is one of the noninvasive techniques that have different applications in the characterization of tissues and the diagnosis of a large number of different diseases.¹ Metabolic states of the cells and conformations of macromolecules, in both quantity and microenvironment, could be reflected by changes of endogenous chromophores that are mainly represented by amino acids, flavin adenine dinucleotide (FAD), and reduced nicotinamide adenine dinucleotide (NADH).²

Both NADH and FAD play key roles in the conversion of energy from acetyl CoA, derived from food molecules, to adenosine triphosphate (ATP), the most important molecule for capturing free energy in cells. NADH functions as a coenzyme and is one of the primary electron donors, while FAD cofactor is among the electron acceptors in electron transport chain (ETC) of the oxidative phosphorylation. These metabolic electron carriers exist in two physiological forms, free and protein bound, and upon binding to mitochondrial membrane proteins they are associated with energy generation. NADH molecules carry away the energy liberated in these reactions in the form of a hydride ion, a hydrogen atom with two electrons.³ When the hydride ion is lost, NADH becomes NAD⁺. FAD is also

used to carry energy away from the citric acid cycle. FAD removes two hydrogen atoms from the four-carbon compound succinate and becomes FADH₂. Thus, monitoring the ratio between free and enzyme-bound forms of these fluorophores can give an insight into the metabolic state of cells.

The nature of bacterial infections and their influence on cells are of critical interest to researchers in large area of disciplines, such as microbiology, medicine, and drug design. It has been known that enterohemorrhagic *Escherichia coli* (EHEC) and enteropathogenic *Escherichia coli* (EPEC) are important human pathogens that cause persistent diarrhea, especially in young children.⁴ EHEC and EPEC have similar but unique 35-kb pathogenicity island, the locus of enterocyte effacement (LEE), which contains genes critical for the bacterial virulence. Both of them colonize the intestinal mucosa and induce attaching and effacing (A/E) lesions, which are characterized by the destruction of intestinal microvilli and formation of polymerized actin structure beneath the bacterium called pedestal.^{5,6} To do so, the bacterial LEE islands encode type III secretion systems (TTSS) to deliver bacterial effector proteins into host cells to subvert host cell signaling pathways. One of the effector proteins of TTSS, Tir, is translocated into the host cell membrane and consequently interacts with a bacterial outer membrane protein, intimin, and this interaction triggers cytoskeletal rearrangements.⁷ Moreover, EHEC and EPEC would modulate the survival of host cell by interfering with pro- and antiapoptotic

*These authors contributed equally to this work.

Address all correspondence to: Fu-Jen Kao, National Yang-Ming University, Institute of Biophotonics, 155 Linong Street, Section 2, Taipei 11221, Taiwan; Tel: +886 2 28267336; Fax: +886 2 28235460; E-mail: fjkao@ym.edu.tw

pathways. According to previous studies, EPEC could induce extrinsic and intrinsic apoptotic pathways by bacterial surface bundle-forming pil^{8,9} and effector proteins, such as EspF and Map.^{10–14} EPEC also antagonizes proapoptosis by delivering antiapoptosis effectors, such as EspZ and NleH, to promote cell survival.¹⁵ Therefore, EPEC-infected cells only exhibit early-phase apoptotic features (expression of phosphatidylserine on the cell surface and DNA cleavage) and features of late-phase apoptosis (cell shrinkage, membrane blebbing, and nuclear condensation) are not observed.^{16,17} All these studies suggest a change of the cellular metabolism as a result of bacterial infection.

NADH and FAD are intrinsically excitable to generate fluorescence, but their respective redox partners, NAD⁺ and FADH₂, are not.¹⁸ Strong NADH absorption takes place in the ultraviolet (UV) range, with a maximum wavelength at around 360 nm. The resulting emission maximum is at around 460 nm. As a comparison, FAD absorbs in the blue, with absorption maximum at around 470 nm and emits green/yellow, with an emission maximum at around 540 nm.¹⁹ The emission spectra of free and protein-bound forms of these fluorophores differ slightly and the overlapping endogenous spectra make it difficult to distinguish between individual components.

In addition to measurements of the fluorescence intensity of NADH and FAD, further information on the metabolic state of a biological sample can be obtained from the fluorescence lifetimes of NADH and FAD by the use of fluorescence lifetime imaging microscopy (FLIM). The method is based on the measurement of the average time fluorescent molecules spent on the excited state levels.²⁰ The values of fluorescence lifetime for a given chromophore is calculated by fitting a measured fluorescence decay. Among other parameters, fluorescence lifetime of a given chromophore can be affected in the proximity of a quencher and/or energy transfer. This makes FLIM a useful technique for probing molecular conformation. In particular, free and bound states of NADH and FAD have well-separated values of fluorescence lifetimes, caused by quenching by adenine moiety at folding.²¹ As NADH binds to a protein, its lifetime increases from ~400 ps to ~2.5 ns.^{22–25} The fluorescence lifetime of free FAD is thought to be around 2.3 ns.²⁶ However, a number of short lifetime components, on the order of tens of picoseconds, have also been reported.^{27,28} The fluorescence lifetime of bound FAD is 0.3 ns, which is lower than that of free FAD.²⁹ The fluorescence lifetime values measured from FAD in our studies differ from some of the publications, but are in agreement with others. Spectral properties of these molecules seem to vary between different tissues and cell cultures. Fitting the fluorescence decay of either NADH or FLIM to a double exponential model may give also an insight into the relative concentration of these coenzymes functional states (noted as a_1 and a_2). As NADH binds to a protein complex on mitochondrial inner membrane, it donates an electron, which, passed through several other protein complexes, called electron transfer chain, contributes to the hydrogen protons pumping to the intermembrane space, development of electromotive force, downhill flow of protons through the ATP synthase, and as a result, phosphorylation of ADP. NADH binding then can be directly associated with ATP synthesis and correlated with the metabolic activity of a cell.

Molecular dynamics that elucidates the bioenergetics of cells in culture allows proper characterization of the range of the free to bound changes of NADH/FAD in normal state. This provides

a baseline for studying cellular pathophysiology. The metabolic mapping in cell culture by means of FLIM has been demonstrated earlier.^{30,31} In this study we used FLIM to investigate changes in cellular metabolism during early apoptosis caused by EHEC infection and the results are compared with the FLIM data obtained from the staurosporine (STS)-treated cells.

2 Materials and Methods

2.1 Sample Preparation

Cervical carcinoma HeLa cells were seeded at a concentration of 3×10^5 cells/cm² on 24-mm-diameter round glass cover slips (Deckglaser) coated with 100 µg/ml poly-L-lysine (Sigma). Coverslips were kept in 3.5 cm dishes filled with growth media [(DMEM) supplemented with 10% fetal bovine serum] and incubated in humidified atmosphere at 37°C with 5% CO₂ overnight. The cells were then washed with phosphate-buffered saline (PBS) and replenished with phenol red-free DMEM (Gibco BRL). Infection to the cells was accomplished by overnight incubation with wild-type (WT) EHEC O157:H7 (ATCC 43888) with dilution of 1:50 with further incubation at 37°C in 5% CO₂ incubator for 1 h. After infection, cover slips were washed with PBS and then overlaid with phenol red-free DMEM for another 3 and 5 h for observations of NADH/FAD autofluorescence and pedestal formation, respectively.

For the treatment with apoptosis inducer, we used staurosporine (STS) (Sigma) at a concentration of 4 µM as a medium dose.^{32,33} HeLa cells (3×10^5) were similarly cultured as described above. The cells were then washed with PBS and replenished with phenol red-free DMEM containing 4 µM STS at 37°C in 5% CO₂ incubator for 1 h, and autofluorescence observed for 3 h.

2.2 Flow Cytometry

The procedure of sample preparation is similar to that of autofluorescence observation. To facilitate the flow cytometry measurement, 1.2×10^6 of HeLa cells were used. After the infection or the STS treatment, cells were harvested and stained with FITC annexin V or 7-amino-actinomycin (7-AAD) (BD Biosciences). The percentage of the annexin V-stained or the 7-AAD-stained cells was analyzed by flow cytometer (BD FACS Canto) within 1 h.

2.3 Imaging

For both NADH and FAD FLIM observations, infected and control cells were excited by a mode-locked Ti:Sapphire Mira F-900 laser (Coherent), pumped by a solid-state frequency-doubled 532 nm Verdi laser (Coherent) and operating in two-photon mode at 740 and 860 nm, for the excitation of NADH and FAD, respectively. The excitation beam was coupled to the FV300 scanning unit (Olympus)³⁴ with the scanning speed set by a function generator (AFG310; Tektronix) for the image acquisition optimization. The beam was focused on the sample with a 60×1.45 NA plan apochromat oil immersion objective (Olympus). An average laser power of ~4 mW (power at focus is much more meaningful) above the objective was used for imaging in order to prevent photo damage of the cells.³⁵ Imaging was conducted on a modified inverted Olympus microscope (IX 71) completed with incubator (H-201, Oko-Lab) to maintain the viable physiological and physicochemical conditions of 37°C and 5% CO₂. To match the spectral characteristics

of excited molecules we used band-pass filters of 447 ± 30 nm and 520 ± 60 nm (Semrock) for detection of NADH and FAD autofluorescence, respectively.³⁶ For rejection of the excitation light at 740 nm, we used an additional short-pass and infrared (IR) cut-off filters. The autofluorescence from the cells has been detected by a cooled GaAsP PMT (H7422-P40; Hamamatsu Photonics). Time-resolved data acquisition has been conducted by time-correlated single photon counting system (SPC-830; Becker&Hickl).³⁷ All FLIM images were taken at 256×256 pixels resolution with the accumulation time of 600 s for collecting enough photon counts for statistics data analysis.

2.4 Data Analysis

The analysis of collected data has been done with the SPCImage (v. 2.8) software package (Becker & Hickl GmbH).³⁸ Lifetime calculation from the multiexponential decay was performed by mathematical convolution of a model function and the instrument response function (IRF) with fitting to the experimental data. Lifetimes from the composite decays of both NADH and FAD were derived by convolution of an IRF, I_{instr} , with a double-exponential model function, defined in Eq. (1), with offset correction for the ambient light and/or dark noise I_0 to obtain calculated lifetime decay function $I_c(t)$ in Eq. (2):

$$F(t) = a_1 e^{-t/\tau_1} + a_2 e^{-t/\tau_2}, \quad (1)$$

$$I_c(t) = \int_{-\infty}^{\infty} I_{\text{instr}}(t) \{I_0 + F(t)\} dt(2). \quad (2)$$

Here $a_1 e^{-t/\tau_1}$ and $a_2 e^{-t/\tau_2}$ represent the contributed fluorescence decays from short and long lifetime components of NADH, respectively. τ_1 and τ_2 are their corresponding lifetime constants; a_1 and a_2 are the corresponding relative amplitudes. I_{instr} was measured experimentally with the PPLN crystal at 370 nm and 480 nm for NADH and FAD imaging, respectively (the second harmonic of 740 nm and 860 nm from the Ti:Sapphire laser). Taking into account that IRF is a limiting factor in fluorescence lifetime measurements, deconvolution was applied to all decays in an image to overcome this problem.

The decay FWHM in both cases thus obtained was equal to ~ 320 ps. The average lifetime was calculated as an amplitude-weighted of the two lifetime components:

$$\tau_a = \frac{a_1 \tau_1 + a_2 \tau_2}{a_1 + a_2}. \quad (3a)$$

The model parameters (i.e., a_i and τ_i) were derived by fitting the decay $I_c(t)$, from Eq (2), to the actual data $I_a(t)$ through minimizing the goodness-of-fit function defined in Eq (3b) using the Levenberg-Marquardt search algorithm.

$$\chi_R^2 = \frac{\left\{ \sum_{k=0}^n \frac{[I_a(t) - I_c(t)]^2}{I_a(t)} \right\}}{(n - p)}. \quad (3b)$$

Here n is the number of the data (time) points (equal to 256), and p is the number of the model parameters. The ratio of a_1 and a_2 is the best indicator of free and protein-bound states of NADH and FAD and can be used to indicate the status and changes in cellular metabolism.³⁰

3 Results and Discussion

Mitochondria-mediated apoptosis involves a series of biochemical events including mitochondrial membrane potential (MMP) disruption, cytochrome C release, and various caspases' activation. It has been previously reported that average NADH fluorescence lifetime exhibited a significant increase after 1 μ M STS-induced mitochondria-mediated apoptosis.³⁰ The results suggest that the increment of NADH fluorescence lifetime indicative of an increase of the bound NADH relative concentration could be related to changes of mitochondrial function and may be used as noninvasive optical probes for early detection of programmed cell death.

In order to eliminate bacterial autofluorescence that may interfere with the observation of cellular NADH and FAD autofluorescence, nonattached bacteria were washed away after 1 h of infection prior to NADH and FAD autofluorescence detection for another 3 to 5 h. In a parallel experiment, infectivity of EHEC was examined by staining bacteria and cellular actin for the pedestal formation. Figure 1 shows that EHEC can adhere and contributes to the formation of pedestal structure.

3.1 Bacteria Can Induce Early Stage of Apoptosis

To investigate whether EHEC also affects cellular signaling, such as apoptosis, HeLa cells were separately infected with EHEC, an EHEC mutant with one of the TTSS gene (*escN*) deletion, JM109 (a nonpathogenic K-12 *E. coli* strain), and UV-inactivated JM109. After infection, the cells were then measured for the apoptotic percentages by flow cytometry with Annexin V and 7-AAD staining. By doing so, the infected cells were discriminated into viable (Annexin V^{neg}/7-AAD^{neg}), early apoptotic cells (Annexin V^{pos}/7-AAD^{neg}), and late apoptotic cells or dead cells (Annexin V^{pos}/7-AAD^{pos}). In addition, HeLa cells were treated with 4 μ M STS as a known apoptosis positive control. After 4 h of infection, 66.5% and 12.1% of the EHEC-infected cells were found to be at early and late apoptotic phases, respectively. Notably 29.1% and 9.7% of noninfected cells at early and late stage of apoptosis were probably due to the fact that some damage occurred to cellular membrane during the detachment process. In contrast, the STS-treated cells yielded a lower percentage of the early apoptotic cells (53.4%) than that of the EHEC infected cells, whereas the percentage of cells stained at the late apoptotic phase (22.7%) was higher than that of the EHEC-infected cells. Therefore, these results supported the notion that the EHEC infection induces early apoptosis but slightly inhibits the late apoptosis. To further investigate whether TTSS is a necessity for apoptotic response

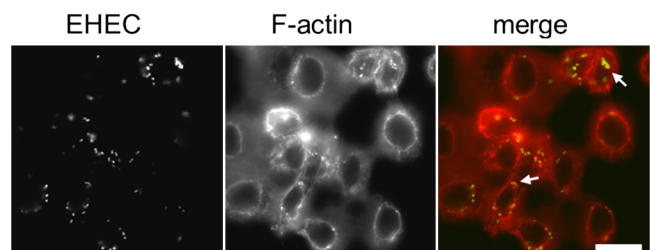


Fig. 1 Pedestal formation after HeLa cells were infected with EHEC for 6 h. Pedestal formations (arrows) were observed by fluorescent microscopy. Bacteria were visualized by staining with an anti-EHEC O-antigen antibody (green); actin was detected by staining with Texas Red Phalloidin (red). The scale bar is 10 μ m.

during the infection, the *escN*-deleted EHEC was used to infect cells, which were analyzed by flow cytometry.³⁹ Figure 2 and Table 1 show that these TTSS-defected bacteria (Δ *escN*) resulted in a lower percentages of apoptotic cells than those of the parental EHEC, suggesting the enhancing effect of TTSS on apoptosis. Furthermore, we used nonpathogenic JM109 and UV-inactivated JM109 as controls such that the effect of live, nonpathogenic bacteria and the lipopolysaccharide (LPS) from the dead bacteria could be evaluated, respectively. Whereas a total of 78.6% of apoptotic cells was associated with the infection with EHEC, only 55.1% of apoptotic cells were associated with that of JM109, and 44.2% from that with the UV-inactivated JM109. These observations consolidate the notion that pathogenic EHEC induce an apoptotic response in host cells, particularly with early apoptotic feature. Percen-

tages of the late apoptotic cell were not significantly altered when compared with that of the control HeLa cells.

Mitochondria have been shown to be essential for cell metabolism and are one of the primary organelles affected by apoptosis. In particular, MMP disruption would lead to the failure of oxidative phosphorylation apoptosis (high ATP).^{40,41} The disruption could also lead to necrosis (low ATP). Our results described above indicate that EHEC induces early apoptotic response in the host cells. Furthermore, a complete, active TTSS of EHEC also enhanced apoptosis.

3.2 Cell Metabolism Perturbations by Infection

Recent studies showed that using multiphoton FLIM of NADH is a powerful tool to study cellular metabolism in living

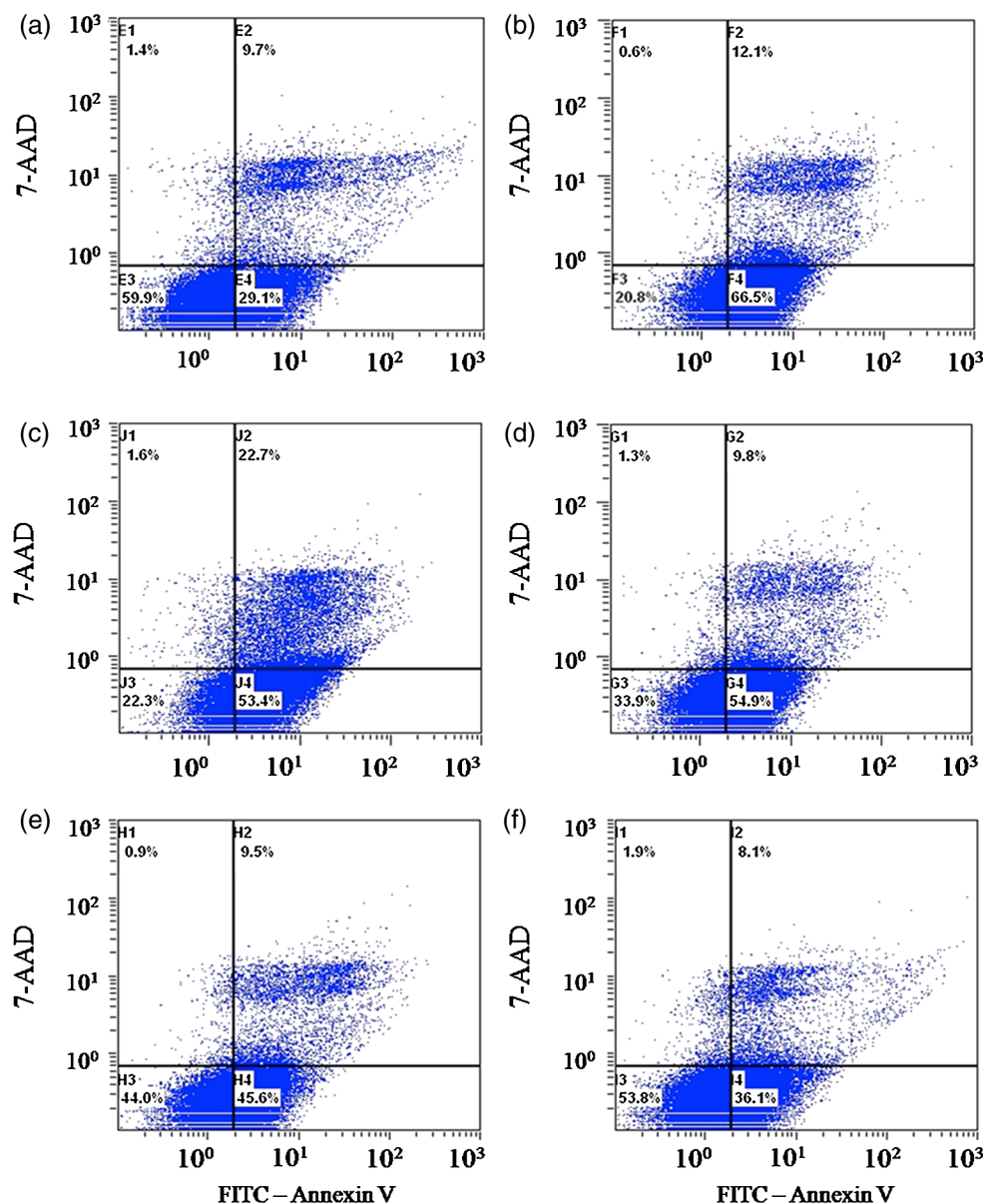


Fig. 2 Flow cytometry data showing apoptosis percentage of HeLa cells upon bacterial infection and STS-treatment. The x and y axes represent the intensity of FITC annexin V and 7-AAD, respectively. The percentage of cells in each cellular state (viable, early apoptotic cells, late apoptotic cells, or dead cells) is shown inside the cross. (a) HeLa cells only. (b) EHEC infected cells. (c) STS-treated cells. (d) Cells infected with *escN*-deleted EHEC. (e) JM109-infected cells. (f) cells treated with UV-inactivated JM109.

Table 1 Percentage of the apoptosis probability in HeLa cells only, WT EHEC infected, STS-treated and Δ escN EHEC infected, JM109 infected, and UV-inactivated JM109 infected HeLa cells.

Stages	Stains					
	HeLa cells only	WT EHEC	STS	Δ escN EHEC	JM 109	UV-inactivated JM 109
Early apoptosis	29.1%	66.5%	53.4%	54.9%	45.6%	36.1%
Late apoptosis	9.7%	12.1%	22.7%	9.8%	9.5%	8.1%
Total apoptosis	38.8%	78.6%	76.1%	64.7%	64.7%	44.2%

cells.^{29,42} NADH fluorescence lifetimes differ distinctly in cytosol, mitochondria and nucleus in single cell.^{43–45} Different bindings of NADH to proteins may result in different NADH fluorescence lifetimes that reflect the diverse physiological functions in these cellular compartments. To reveal metabolic changes in cells upon infection, cultured HeLa cells were continuously imaged during the 3 h after incubation with EHEC. Control noninfected HeLa cells were also imaged under the same conditions. We used τ_a from Eq. (3) along with the ratio of relative contributions from free and bound species (a_1/a_2) of both NADH and FAD to indicate the cellular metabolic states²⁹ (Fig. 3).

a_1/a_2 ratio of free and bound form of NADH (3.46 ± 0.20) was observed at the initial phase of infection [Fig. 3(b)]. During the next 2 h of imaging, this ratio increased gradually up to 3.99 ± 0.30 at the third hour. Control value of a_1/a_2 is equal to 4.11 ± 0.38 . Similar results of a_1/a_2 ratio of NADH in mouse embryonic epithelial fibroblast NIH 3T3 cells have been reported by Buryakina et al.⁴⁶

Most of the free energy released during oxidation of glucose to CO_2 is retained in NADH and FADH_2 generated in glycolysis and the citric acid cycle. During respiration, electrons are released from NADH and FADH_2 then transferred to O_2 [Eqs (3) and (4)]:

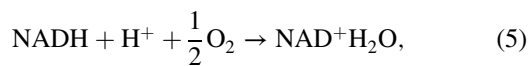


Figure 3(b) shows the relative intensity ratios of free and protein-bound FAD in HeLa cells, which exhibits opposite dynamics of changes in a_1/a_2 ratio in NADH during the same time of bacterial infection. The values of a_1/a_2 both of NADH and FAD are represented in Fig. 3(c). The increase of a_1/a_2 ratio of NADH and its decrease in FAD during infection are also illustrated in Fig. 3(d) and 3(e), respectively.

a_1/a_2 ratio of NADH is increasing with infection time and the highest value is for control. In Fig. 3(b), a_1/a_2 ratio of FAD is decreasing with time and the lowest value is detected for the control. So in the case of NADH, after 1 h of infection protein-bound component increases, if free component is assumed unchanged. The shift of both NADH and FAD a_1/a_2 ratios to their control values at 3 h could be also used as the opposite trend of changes in time for donor coenzyme and acceptor co-factor.

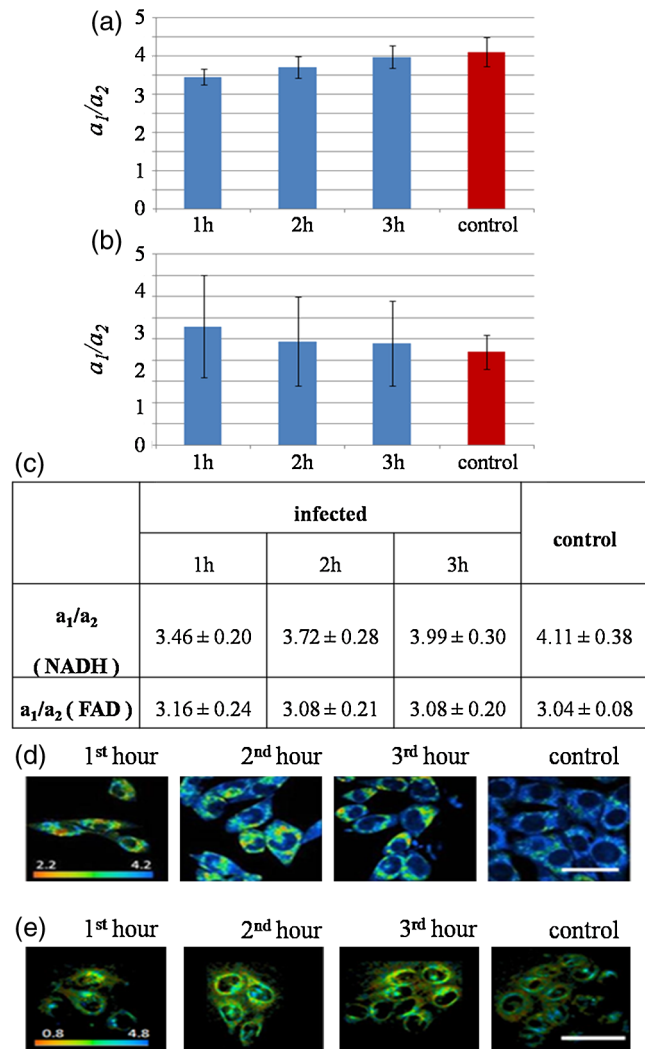


Fig. 3 Bar charts for the peak values of a_1/a_2 ratio histograms, averaged for each hour after the treatment and control. (a) Time-lapse dynamics of NADH a_1/a_2 ratio measured from HeLa cells infected by EHEC. (b) Time-lapse dynamics of FAD a_1/a_2 ratio measured from HeLa cells infected by EHEC. (c) Table of hourly averaged summaries from at least five measurements of the peak values from NADH and FAD a_1/a_2 distribution histograms. (d) Representative color-coded FLIM images of the dynamic of the a_1/a_2 ratio of NADH. (e) Representative color-coded FLIM images of the dynamic of the a_1/a_2 ratio of FAD. The error bar represents the standard deviation for the ratio measurements. The scale bar is 100 μm .

To assure that an infection results in cell apoptosis, we used STS, a well-known apoptosis inducer to treat the cells. At the first hour, we observed a high value of the mean lifetime of NADH at 1315 ± 54.77 ps that decreased to 1255 ± 20.91 ps at the third hour. Control sample has a value of 1364 ± 8.36 ps, which is higher than those of the infected samples even at the first hour [Fig. 4(a)].

Under similar experimental conditions, STS-treated cells exhibit a slight decrease of mean lifetime of NADH, from 3552 ± 209 ps at the first hour of infection to 3184 ± 87 ps at third hour, which is still higher than the mean lifetime value of the control sample [Fig. 4(b)].

Free and protein-bound components lifetimes (τ_1 and τ_2) have peaks at ~ 600 and ~ 3000 ps, respectively. These results are close to the previously published lifetime values of free ~ 400 to 500 ps and bound NADH ~ 2000 to 3000 ps.^{19,47} Broader distribution of τ_2 may be attributed to the wide distribution of lifetimes of NADH molecules bound to different proteins. Observed dynamics of dramatically high mean lifetime and its decrease in time upon both the addition of STS and infection was caused by the changes of the free and bound species' relative fractions. The lifetime shift could be attributed to the fact that free NADH fraction is diminished to an extent after both treatments. Gradual increase exhibited by a_1 (data not shown) corresponds to the moving of average lifetime to the lower values at the time-lapsed imaging.

It has been reported previously by Gukassyan et al.³⁰ that upon the addition of $1 \mu\text{M}$ STS, cells exhibit a rapid and dramatic increase of the average lifetime from 1360 ± 24 ps to 3601 ± 56 ps. STS treatment at the first hour in our experiment resulted in a similar lifetime value of 3552 ± 208.6 ps. The value was decreasing during the next 2 h. Obviously, bacterial infection and the STS-treatment resulted in a similar trend of decreasing lifetimes with time.

The increase in the average lifetime of NADH fluorescence after STS-induced apoptosis may be attributed to the higher portion of bound NADH relative to that of free NADH. An

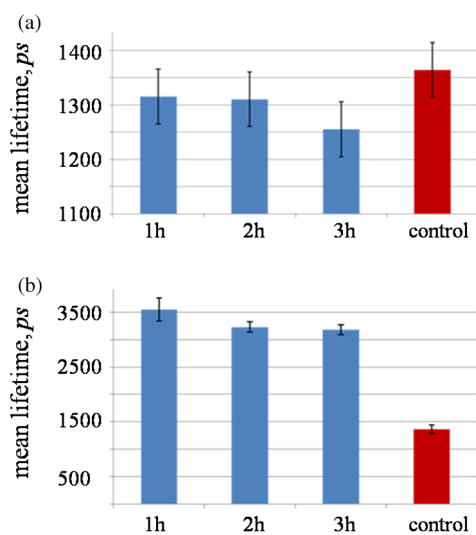


Fig. 4 Column bar chart for the peak values of mean lifetime histograms, averaged for each hour after the treatment and control. (a) Mean lifetime of NADH of HeLa cells infected by EHEC. (b) Mean lifetime of HeLa cells treated by $4 \mu\text{M}$ of STS. The error bar represents the standard deviation for the ratio measurements.

additional explanation to account for our results is that the bound NADH lifetime increases when compared to free NADH lifetime. Observed decrease in time during possible apoptosis in both cases of STS-treatment and bacterial infection suggests that there may exist some fast dynamics of NADH lifetime in the first hour with further decrease, which, however, could not be detected more properly and are a subject for future studies.

High fluorescence and metabolically active perinuclear ring represents a subpopulation of mitochondria that are mobilized in response to the apoptotic stimulus and may provide the energy required to execute the last step of apoptosis. Infected cells did not give the morphology changes mentioned above during 3 h of infection as the STS treatment. However, the fluorescence was becoming intense as the cells were undergoing a longer time of infection.

During early apoptosis there is some loss of mitochondrial function, so that mean lifetime increases, because of free lifetime component of NADH remains constant and the protein-bound one increases. Bound NADH lifetime increases, assuming that the free NADH lifetime does not change, due to microenvironment changes that NADH binds to different enzymes during early apoptosis. Another possible reason is that the portion of bound NADH in total amount of NADH is higher than that of free NADH, assuming their lifetimes remain the same. It can be observed because some NADH may bind to different enzymes, so that lifetime distribution could become broader.

The most common optical method for metabolic imaging is the redox ratio, which is the ratio of the fluorescence intensity of FAD and NADH. To calculate redox ratio we exported values of intensity in each pixel in useful FOV from both FAD and NADH by using included tool in SPCImage software before obtaining the lifetime images and calculated the ratio of initial intensities. This ratio provides relative changes in the oxidation-reduction state in the cell. We also monitored the redox ratio of HeLa cells in both infection with bacteria and STS treatment (Fig. 5).

Conversion of NADH fluorescence intensity values to absolute concentration values is not straightforward. Therefore, this

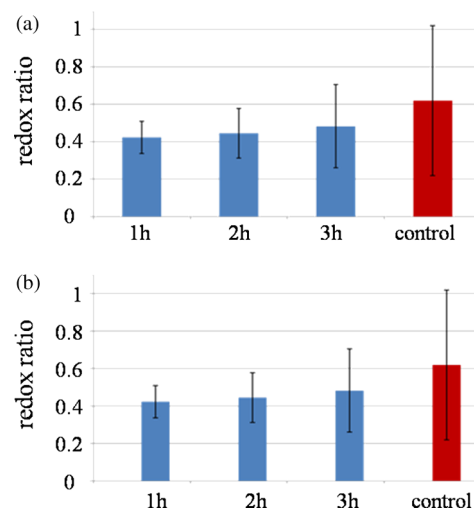


Fig. 5 Time-lapsed dynamics of redox ratio in HeLa cells. (a) Infection with EHEC. (b) Treatment with $4 \mu\text{M}$ STS. The error bar represents the standard deviation for the ratio measurements.

situation poses a limitation for NADH FLIM. In addition, the fluorescence decay parameters of the phosphorylated and nonphosphorylated forms of reduced NAD⁺ are similar and indistinguishable. However, estimations of the cellular concentrations suggest that a substantial part of the cellular fluorescence originates from NAD(P)H rather than from NADH.³⁹ The influence the NADPH on the signal detected in the 740 nm-excited spectral range is neglected. Early reports have identified lower quantum yield of NADPH at a factor of 1.25 to 2.5 when compared to that of NADH.³⁰ The concentration of reduced NADH in cells is fivetimes greater than that of NADPH. There is still NAD(P)H signal, which hardly can affect the fluorescence of interest.⁴⁸ Complex analysis of a mixture of multiple fluorophores, featuring multiexponential decays overlapping each other both spectrally and in their lifetimes and spectral unmixing can become possible to help the situations.

There is also some portion of the FAD spectrum covered with the filter used,⁴⁹ but given that measured at the maximum of the spectra FAD signal was smaller than NAD(P)H, we believe that there is little-to-no influence on the NADH fluorescence lifetime values.

Nevertheless, a reliable analysis of the NAD(P)H fluorescence in the early phase of infection could not be performed. The use of NADH autofluorescence is still needed to provide a clue to the mapping of metabolic changes during early apoptosis caused by infection.

4 Summary

FLIM performed on NADH and FAD is able to properly characterize both physiological and pathological states of live cells by mapping of cellular metabolic states. This technique is important to understand and reflect the correlation of NADH and FAD lifetime dynamics with the biological processes in cells and can be efficiently used to distinguish lifetime differences in normal and pathological specimens.

The combination of fluorescence redox ratio and lifetime imaging at high resolution might potentially provide a tool for understanding the morphological and metabolic changes in cell culture. These observations help to unravel the early studies of apoptosis in case of bacterial infection and could be used as a guide for the time-gated and steady-state fluorescence methods for the clinical detection of diseases. Moreover, the changes in lifetime and relative intensities ratios of FAD as opposed to NADH at early apoptosis make the technique able to demonstrate the roles and functions of enzymes and co-factors in cells by means of fluorescence lifetime signatures.

Two-photon FLIM also reveals new insights into the crosstalk between host and pathogen metabolism and suggests that pathogenic *E. coli* (EHEC) induced changes in subcellular NADH in such a way as to directly interfere with signaling pathways that are involved in cellular survival and longevity. Understanding how host cell metabolism reacts on extracellular pathogens and metabolic profiling of infected cells by FLIM of NADH will be an invaluable tool that complements established large-scale genomic and proteomic approaches.

To make the study more clear and solid, more experiments should be done. To prove the possible apoptosis in infected cells, ATP level both in control and treated cells should be measured. Imaging of NADH in HeLa cells infected with lower and higher bacteria concentration is important also to reveal the real changes in metabolism caused by the infection of *E. coli*. Not only *E. coli*, but also other types of bacteria should be

used to infect the cells prior the imaging of NADH lifetime in HeLa cells to reflect the fact of a_1/a_2 changes during different infection time. Other cell lines could be also informative to reveal changes in metabolism by means of NADH lifetime perturbations by FLIM.

Acknowledgments

This work is generously supported by the National Science Council under grants 98-2112-M-010-001-MY3, 97-2112-M-010-002-MY3, 99-2627-M-010-002, in part by the UST-UCSD International Center of Excellence in Advanced Bioengineering sponsored by Taiwan National Science Council I RiCE Program under grant NSC-100-2911-I-009-101 and a grant from Ministry of Education, Aim for the Top University Plan.

References

1. Y. Wu and J. Y. Qu, "Combined depth- and time-resolved autofluorescence spectroscopy of epithelial tissue," *Opt. Lett.* **31**(12), 1833–1835 (2006).
2. Y. Wu et al., "Depth-resolved fluorescence spectroscopy reveals layered structure of tissue," *Opt. Express* **12**(14), 3218–3223 (2004).
3. B. Alberts et al., *Molecular Biology of the Cell*, 5th ed., Garland Science, New York (2008).
4. M. Levine and R. Edelman, "Enteropathogenic *Escherichia coli* of classic serotypes associated with infant diarrhea: epidemiology and pathogenesis," *Epidemiol. Rev.* **6**(1), 31–51 (1984).
5. T. Ide et al., "Differential modulation by Ca²⁺ of Type III secretion of diffusely adhering enteropathogenic *Escherichia coli*," *Infect. Immun.* **71**(4), 1725–1732 (2003).
6. T. K. McDaniel and J. B. Kaper, "A cloned pathogenicity island from enteropathogenic *Escherichia coli* confers the attaching and effacing phenotype on *E. coli* K-12," *Mol. Microbiol.* **23**(2), 399–407 (1997).
7. M. De Grado, "Identification of the intimin-binding domain of Tir of enteropathogenic *Escherichia coli*," *Cell. Microbiol.* **1**(1), 7–17 (1999).
8. M. Abul-Milh et al., "Induction of epithelial cell death including apoptosis by enteropathogenic *Escherichia coli* expressing bundle-forming pili," *Infect. Immun.* **69**(12), 7356–7364 (2001).
9. A. R. Wong, "Enteropathogenic and enterohaemorrhagic *Escherichia coli*: even more subversive elements," *Mol. Microbiol.* **80**(6), 1420–1438 (2011).
10. J.-Ph. Nougayrede and M. S. Donnenberg, "Enteropathogenic *Escherichia coli* EspF is targeted to mitochondria and is required to initiate the mitochondrial death pathway," *Cell. Microbiol.* **6**(12), 1097–1111 (2004).
11. V. Viswanathan et al., "Enteropathogenic *E. coli*-induced barrier function alteration is not a consequence of host cell apoptosis," *Am. J. Physiol. Gastrointest. Liver Physiol.* **294**(5), G1165–G1170 (2008).
12. P. Dean et al., "The enteropathogenic *E. coli* effector EspF targets and disrupts the nucleolus by a process regulated by mitochondrial dysfunction," *PLOS Pathog.* **6**(6), e1000961 (2010).
13. A. Holmes et al., "The EspF effector, a bacterial pathogen's Swiss Army Knife," *Infect. Immun.* **78**(11), 4445–4453 (2010).
14. C. Hemrajani et al., "NleH effectors interact with Bax inhibitor-1 to block apoptosis during enteropathogenic *Escherichia coli* infection," *PNAS* **107**(7), 3129–3134 (2010).
15. J. Crane et al., "Host cell death due to enteropathogenic *Escherichia coli* has features of apoptosis," *Infect. Immun.* **67**(5), 2575–2584 (1999).
16. J. Crane et al., "Role of EspF in host cell death induced by enteropathogenic *Escherichia coli*," *Cell. Microbiol.* **3**(4), 197–211 (2001).
17. M. R. Duchon, A. Surin, and J. Jacobson, "Imaging mitochondrial function in intact cells," *Methods Enzymol.* **361**, 353–389 (2002).
18. B. Chance et al., "Oxidation-reduction ratio studies of mitochondria in freeze-trapped samples. NADH and flavoprotein fluorescence signals," *J. Biol. Chem.* **254**(11), 4764–4771 (1979).
19. J. R. Lakowicz, *Principles of Fluorescence Spectroscopy*, Plenum Press, New York (1999).

20. K. Blinova et al., "Distribution of mitochondrial NADH fluorescence lifetimes: steady-state kinetics of matrix NADH interactions," *Biochemistry* **44**(7), 2585–2594 (2005).
21. A. J. W. G. Visser and A. V. Hoek, "The fluorescence decay of reduced nicotinamides in aqueous solution after excitation with a UV-mode locked laser," *J. Photochem. Photobiol.* **33**(1), 35–41 (1980).
22. W. R. Zipfel, R. M. Williams, and W. W. Webb, "Nonlinear magic: multiphoton microscopy in the biosciences," *Nat. Biotechnol.* **21**(11), 1369–1377 (2003).
23. A. Gafni and L. Brand, "Fluorescence decay studies of reduced nicotinamide adenine dinucleotide in solution and bound to liver alcohol dehydrogenase," *Biochemistry* **15**(15), 3165–3171 (1976).
24. M. Wakita, G. Nishimura, and M. J. Tamura, "Some characteristics of the fluorescence lifetime of reduced pyridine nucleotides in isolated mitochondria, isolated hepatocytes, and perfused rat liver in situ," *J. Biochem.* **118**(6), 1151–1160 (1995).
25. F. Frischknecht, O. Renaud, and S. L. Shorte, "Imaging today's infectious animalcules," *Curr. Opin. Microbiol.* **9**(3), 297–306 (2006).
26. N. Nakashima et al., "Picosecond fluorescence lifetime of the coenzyme of D-amino acid oxidase," *J. Biol. Chem.* **255**(11), 5261–5263 (1980).
27. P. A. W. Van den Berg et al., "Dynamic conformations of flavin adenine dinucleotide: simulated molecular dynamics of the flavin cofactor related to the time-resolved fluorescence characteristics," *J. Phys. Chem. B* **106**(34), 8858–8869 (2002).
28. D. Chorvat, Jr. and A. Chorvatova, "Multi-wavelength fluorescence lifetime spectroscopy: a new approach to the study of endogenous fluorescence in living cells and tissues," *Laser Phys. Lett.* **6**(3), 175–193 (2009).
29. M. C. Skala et al., "In vivo multiphoton microscopy of NADH and FAD redox states, fluorescence lifetimes, and cellular morphology in precancerous epithelia," *PNAS* **104**(49), 19494–19499 (2007).
30. H. W. Wang et al., "Differentiation of apoptosis from necrosis by dynamic changes of reduced nicotinamide adenine dinucleotide fluorescence lifetime in live cells," *J. Biomed. Opt.* **13**(5), 054011 (2008).
31. V. Ghukasyan and F. J. Kao, "Monitoring cellular metabolism with fluorescence lifetime of reduced nicotinamide adenine dinucleotide," *J. Phys. Chem. C* **113**(27), 11532–11540 (2009).
32. T. Shimizu et al., "A role of reactive oxygen species in apoptotic activation of volume-sensitive Cl⁻ channel," *PNAS* **101**(17), 6770–6773 (2004).
33. E. Maeno, "Normotonic cell shrinkage because of disordered volume regulation is an early prerequisite to apoptosis," *PNAS*, **97**(17), 9487–9492 (2000).
34. V. Ghukasyan et al., "Application of fluorescence resonance energy transfer resolved by fluorescence lifetime imaging microscopy for the detection of enterovirus 71 infection in cells," *J. Biomed. Opt.* **12**(2), 024016 (2007).
35. I.-H. Chen et al., "Wavelength dependent damage in biological multiphoton confocal microscopy: a micro-spectroscopic comparison between femtosecond Ti:sapphire and Cr:forsterite laser sources," *Opt. Quant. Electron.* **34**(12), 1251–1266 (2002).
36. S. H. Huang, A. A. Heikal, and W. W. Webb, "Two-photon fluorescence spectroscopy and microscopy of NAD(P)H and flavoprotein," *Biophys. J.* **82**(5), 2811–2825 (2002).
37. W. Becker, *Advanced Time-Correlated Single Photon Counting Techniques*, Springer Berlin, Heidelberg, New York (2005).
38. V. Ghukasyan et al., "Fluorescence lifetime dynamics of enhanced green fluorescent protein in protein aggregates with expanded polyglutamine," *J. Biomed. Opt.* **15**(2), 016008 (2010).
39. J. Tree et al., "Controlling injection: regulation of type III secretion in enterohaemorrhagic *Escherichia coli*," *Trends Microbiol.* **17**(8), 361–370 (2009).
40. Q. Yu and A. Heikal, "Two-photon autofluorescence dynamics imaging reveals sensitivity of intracellular NADH concentration and conformation to cell physiology at the single-cell level," *J. Photochem. Photobiol. B* **95**(1), 46–57 (2009).
41. N. Pollak, C. Dolle, and M. Zeigler, "The power to reduce: pyridine nucleotides—small molecules with a multitude of functions," *Biochem. J.* **402**, 205–218 (2007).
42. J. J. Lemasters, "Modulation of mitochondrial membrane permeability in pathogenesis, autophagy and control of metabolism," *J. Gastroenterol. Hepatol.* **22**(s1), S31–S37 (2007).
43. E. F. Mason, "Cell metabolism: an essential link between cell growth and apoptosis," *Biochim. Biophys. Acta* **1813**(4), 645–654 (2011).
44. M. Szaszak et al., "Fluorescence lifetime imaging unravels *C. trachomatis* metabolism and its crosstalk with the host cell," *PLoS Pathogens* **7**(7), e1002108 (2011).
45. D. Li et al., "Time-resolved spectroscopic imaging reveals the fundamentals of cellular NADH fluorescence," *Opt. Lett.* **33**(20), 2365–2367 (2008).
46. T. Buryakina et al., "Monitoring cellular metabolism of 3T3 upon wild type *E. coli* infection by mapping NADH with FLIM," *Chin. Opt. Lett.* **8**(10) 931–933 (2010).
47. H. Schneckeburger et al., "Autofluorescence lifetime imaging of cultivated cells using a UV picosecond laser diode," *J. Fluoresc.* **14**(5), 649–654 (2004).
48. A. S. Ladokhin and L. Brand, "Evidence for an excited-state reaction contributing to NADH fluorescence," *J. Fluoresc.* **5**(1), 99–106 (1995).
49. D. Schweitzer, "Quantifying fundus autofluorescence," Chapter 8 in *Fundus Autofluorescence*, N. Lois and J. V. Forrester, eds., pp. 78–95, Lippincott Williams &Wilkins, Philadelphia (2009).